*Oxidation Communications 49, No 3, 444–460* (*2026*)

*Tribochemical interactions on metal and other surfaces in the presence of molecular oxygen or its activated species*

# EXPERIMENTAL AND SURFACE STUDIES ON THE CORROSION INHIBITION EFFECT OF PLATINUM COMPLEX ON COPPER ALLOY IN NITRIC ACID SOLUTION

E. H. ALI, SH. A. SAOUD*, E. J. WAHEED

*Department of Chemistry, College of Education for Pure Sciences, Ibn-Al-Haitham, University of Baghdad, Baghdad, Iraq*
*E-mail*: *shaimaa.a.s@ihcoedu.uobaghdad.edu.iq*

## ABSTRACT

The objectives of this paper was the development of a novel ligand, L, which was achieved in two stages: ligand is synthesised by reducing the result of the reaction between cyclohexane-1,2-diamine and 4-hydroxy-3,5-dimethoxycyclohexane-1-carbaldehyde, followed by the production of the 4,4'-((1E,1'E)-(1,2-phenylenebis(azanylylidene))bis(methanylylidene))bis(2,6-dimethoxyphenol) precursor (P). While studying corrosion inhibition (copper alloy) in acid solution by weight loss, compounds were characterised using $^{1}H$, $^{13}CNMR$ (for ligand (L) and (P)), FT-IR and UV spectra, melting point, molar conductivity, %C, %H and %N, %M, and magnetic susceptibility. The complex's octahedral structure is inferred from the bidentate coordination of the metal ion. The molar ratio of type $[Pt(L)C_{l2}(H_2O)_2]$ seemed to be 1:1(M:L). Using the weight loss method, the corrosion inhibitory effects of the platinum complex on copper alloy in a nitric acid solution (0.5 M $HNO_3$) were studied. Adsorption of inhibitor molecules onto the surface of the copper alloy was the primary mechanism by which corrosion activity was reduced and active sites were blocked. The results demonstrated that the efficacy of inhibition was improved with increasing inhibitor concentrations. The inhibitor had its maximum inhibitory effectiveness of 97.5% at a concentration of 700 ppm. Calculated values of the Gibbs free energy corroborated with the results of adsorption investigations, which showed that the process mostly included physical adsorption and Langmuir adsorption isotherm. The development of protective coatings was validated by scanning electron microscopy analyses of surface morphology.

*Keywords*: copper alloy, platinum complex, corrosion inhibition ,

* For correspondence.

## AIMS AND BACKGROUND

New materials with unique characteristics are desperately needed due to the fast development of science. One example is the requirement for compounds that may delay or prevent damage caused by free radicals; these compounds should have antioxidant capabilities. Free radicals are known to harm cells in certain ways; hindered phenols are particularly intriguing antioxidant molecules and may serve as an important building block for other antioxidant compounds[1]. Two intriguing phenols, vanillin and ortho vanillin, have a broad variety of biological activities, one of which is antioxidant[2]. Metals deteriorate over time due to chemical or electrochemical reactions with their surroundings, a process known as corrosion. Since a lot of money is spent on preventing materials from becoming damaged in manufacturing processes, it has a big impact on the economy[3–5]. Preventing corrosion has several advantages, including a longer lifespan for equipment and less hazardous metal disintegration into the environment. This has positive effects on both the environment and the economy. Researchers have shown a great deal of interest in corrosion studies[6] of copper and its alloys due to the material's large industrial application and economic importance. Electronics, heat exchangers, and electrical conductors are just a few of the many applications of copper. In areas where copper dissolution might occur due to aggressive circumstances, there has been a rise in interest in using platinum complexes as inhibitors. Because of their low production and purification costs, high frequency of active heteroatoms (such as sulphur, nitrogen, and oxygen), and ease of production, inhibitors are promising options[7–9]. Coordination complexes are chemical compounds that have a metallic atom or ion in the middle (the coordination centre) and a network of bound molecules or ions (the ligands) or complexion agents (the agents) around it. Coordination complexes are common in compounds containing metals, particularly those containing transition metals (d-block elements like platinum) in particular. The displacement of water molecules at corrosion sites by inorganic molecules that adsorb onto metal surfaces may slow down anodic and cathodic processes as opposed to the more common inorganic inhibitors[10–14].

The aim of the study was to prepare new complexes and use them as inhibitors for metal corrosion. The bidentate ligand (L) reacted with Pt (ii) to produce a solid complex, which is mentioned in this study along with the production of the ligand and its complex. **Not clear???** Various methods were used for the diagnosis of the produced compounds.

## EXPERIMENTAL

### MATERIALS AND SAMPLE PREPARATION

No refining was done on the elements that were employed; they were of the highest purity (BDH, Fluka, or Merck). Nitrogen, carbon, and hydrogen microelement analyses were performed using an Elemental Analyser EURO EA 3000. The Shimadzu

Uv-16 spectrophotometer was used to record the absorption spectra of complexes in DMSO solutions at room temperature using a quartz cell that was 1 cm in diameter. The Shimadzu-FTIR-8300 unit has been used to record FT-IR spectra in the (4000-400) $cm^{-1}$ region. The sample solution's conductivity was measured in a dimethyl sulphoxide solvent at $10^{-3}$ M concentration and at a room temperature using an EUTECH CON 150 conductivity meter. The magnetic moments ($\mu_{eff}$ B.M) at 25°C were detected using Magnetic Susceptibility Balances made by Sherwood Scientific. The Shimadzu AA-680 apparatus has been used to test the metallic ratios by atomic absorption process. DMSO was used to compute the $^{1}$H-NMR spectra using a 300 MHz NMR spectrometer. The corrosion test was conducted in the chemistry laboratory at the Chemistry Department of the College of Education for Pure Sciences, Ibn Al-Haytham, University of Baghdad. The chlorine concentration in the compounds that were manufactured at the Ibn Sina Company in Baghdad, Iraq was assessed by weight loss assays. Experiments were conducted using the specimen made of copper alloy. Chemical make-ups were as follows (expressed as a percentage of total weight): 99% copper, 0.05% lead, 0.0012% silver, 0.001% nickel, 0.009% zinc, 0.003% aluminum, and 0.0251% iron. Before usage, the samples were degreased with alcohol, cleaned with distilled water, and dried with filter paper. They were cut into circular discs (diameter: 2 cm, thickness: 2 mm). The grinding process used progressively finer grits of emery paper, ranging from 400- to 3000-grit.

*4,4'*-((*1E,1'E*)-(*cyclohexane-1,2-diylbis*(*azanylylidene*))*bis*(*methanylylidene*))*bis*(*2,6-dimethoxyphenol*) (P). The synthesis of this chemical was documented by Shakir R. M et al.[15] In a few fractions, a heated stirring solution of cyclohexane-1,2-diamine (0.1 mol) in 25 ml of absolute ethanol was combined with a solution of 4-hydroxy-3,5-dimethoxycyclohexane-1-carbaldehyde (0.2 mol) in 50 ml of ethanol. The liquid was refluxed with continuous stirring for 5 h after adding four drops of acetic acid. Under lower pressure, the solvent volume was cut in half. The resulting precipitate was washed with cold distilled water after cooling. From the methanol, the resultant chemical crystallised to produce an orange crystal with a melting point of 137–140ºC and an 87% yield; $^{1}$H NMR (Bruker Nuclear Magnetic Resonance spectrometer) (300 MHz, DMSO-$d_6$) δ, ppm; 1.01 (t, 4H, CH2), 1.61 (t, 4H, CH2), 3.79 (s, 12H, O–$CH_3$), 5.20 (bs, 2H, OH), 5.50 (t, 2H, HC-N), 6.84-7.88 (m, 4H, $CH_{aromatic}$), 8.69 (bs, 2H, HC=N). $^{13}$C NMR (75 MHz, DMSO-$d_6$) δ, ppm; 28.21 (4C, CH2), 31.35 (2C, CH2), 56.50 (4C, O–$CH_3$), 61.73 (2C, HC-N), 110.00 (4C, $CH_{aromatic}$), 136.23 (2C, $C_{aromatic}$), 141.61 (2C, C–OH), 149.5811 (4C, C–$OCH_3$), 161.73 (2C, HC=N) (Scheme 1).

*4,4'*-((*cyclohexane-1,2-diylbis*(*azanediyl*))*bis*(*methylene*))*bis*(*2,6-dimethoxyphenol*) (**L**). This chemical was synthesised according to the method described by Shakir et al.[16] The crude precipitate was crystalised from ethanol to afford white amorphous, M.P 259–261ºC, Yield 83%; $^{1}$H NMR (300 MHz, DMSO-$d_6$) δ, ppm; 1.57–1.99 (m, 8H, $CH_2$), 3.88 (s, 12H, $OCH_3$), 4.65 (s, 4H, 2× $CH_2$N), 4.99 (2H, 2×HC–N), 5.25 (2H, 2×NH), 5.52 (2H, 2×OH), 7.332–7.86 (m, $CH_{aromatic}$). $^{13}$C NMR (75 MHz, DMSO-$d_6$)

δ, ppm; 27.22 (4C, $CH_2$), 31.06 (2C, $CH_2$), 48.72 (2C, $CH_2N$), 56.50 (4C, O–$CH_3$), 61.73 (2C, HC–N), 110.00 (4C, $CH_{aromatic}$), 136.23 (2C, $C_{aromatic}$), 141.61 (2C, C–OH), 149.5811 (4C, C–$OCH_3$) (Scheme 1).

Scheme 1
General synthetic rout of compounds **P** and **L**

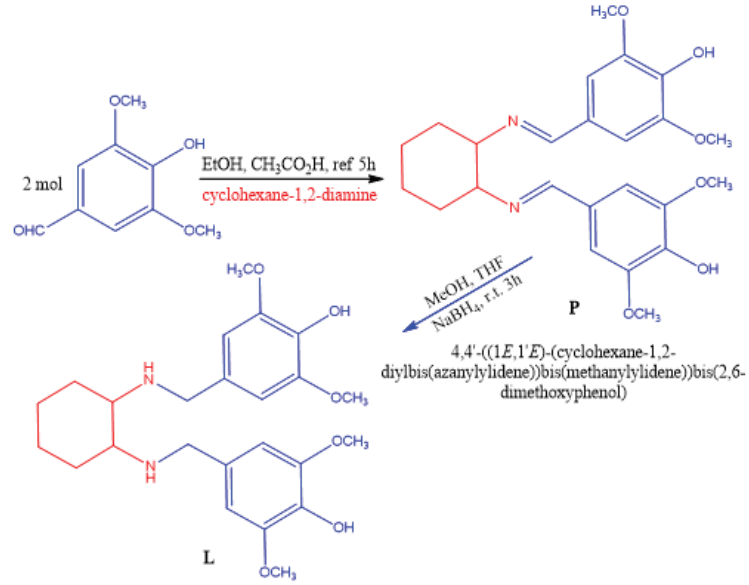


## SYNTHESIS OF THE PLATINUM COMPLEX

The platinum complex (Fig. 1) was prepared with a molar ratio of (1:1) (M:L) using a 100-ml round flask by adding 0.45 g (1 mmol) of platinum salt ($K_2PtCl_4$) dissolved in 10 m ethanol to the ligand solution (L) resulting from dissolving (0.72 g, 1 mmol) in 10 ml) ethanol and leave the mixture at a temperature of 70°C with continuous stirring and reflux for 3 h. The solution was filtered to obtain the brown precipitate. It was washed several times with $H_2O$ distilled and $(C_2H_5)_2O$ and re-crystallised with $CH_3OH$ absolute. Then the percentage of the product and the melting point were determined as 85% and 220-222°C, respectively[17,18].

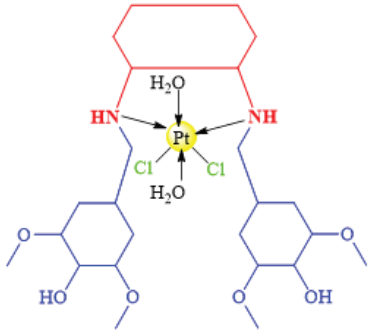


**4,4'-((cyclohexane-1,2-diylbis(azanediyl)) bis(methylene))bis(2,6-dimethoxycyclohexan-1-ol) (L)**

**Fig. 1**. Synthesis of the platinum complex

## WEIGHT LOSS MEASUREMENTS

Weight loss experiments have been implemented in 0.5 M $HNO_3$ solutions with and without different concentrations of inhibitors (500–700 ppm). Immersion tests were conducted for 3 h at various temperatures (25–55°C). After exposure, the specimens were cleaned, dried, and reweighed. Each measurement was repeated three times to ensure accuracy.

Inhibition efficiency (%), corrosion rate (CR) and surface coverage (θ) have been evaluated by means of the following standard equations:

$$\eta\ (\%) = ((i_{corr} - i_{corr(inh)})/i_{corr}) \times 100, \quad (1)$$

where $i_{corr}$, $i_{corr(inh)}$ represent the corrosion current densities as measured when inhibitors are present and when they are not, respectively.

$$\theta = (CR_o - CR_i)/CR_o, \quad (2)$$

where $CR_o$ and $CR_i$ stand for the corrosion rates with and without the inhibitor, respectively.

$$CR_{(mdd)} = (w_o - w_i)/(A\ t), \quad (3)$$

where $w_o$, $w_i$ are the milligram weight losses of the copper alloy with and without inhibitors, respectively; $K$ – the surface covering of the inhibitor, and $A$ – the surface coverage of the outer layers of the specimens. The amount of days counted is what determines the time spent underwater[19].

## RESULTS AND DISCUSSION

A new compound, 4,4'-((cyclohexane-1,2-diylbis(azanediyl))bis(methylene)) bis(2,6-dimethoxyphenol) (**L**), was successfully synthesised from the reaction of 4,4'-((1E,1'E)-(cyclohexane-1,2-diylbis(azanylylidene))bis(methanylylidene))bis(2,6-

dimethoxyphenol) (**P**) as Schiff base[20] with sodium borohydride in the presence of tetrahydrofuran as reduction agent[21] in (T.H.F) and methanol (MeOH), [1:1] as a solvent, according to the first scheme of the broad synthetic pathway. The structures that were generated were validated by the FTIR, $^{1}$H NMR, and $^{13}$C NMR analyses (Figs 2–5). A new band at 3324 $cm^{-1}$ for the two NH groups appeared in the FTIR spectra of compound **L**, which was obtained by reducing compound **P**. The band of the imine group (CH=N) disappeared. Compound **L**'s chemical formula was also validated by $^{1}$H NMR data. In addition to the imine group vanishing, the spectrum reveals the appearance of a new singlet peak at 4.65 ppm, which is attributable to the reduction of the two-imine group to two $CH_2$-N groups and the integration of four protons. The $^{13}$C NMR data corroborated the structures determined by the FTIR and $^{1}$H NMR. The chemical shifts seen in the $^{13}$C NMR spectrum corroborate the predicted carbon configuration of compound **P** and validate compound **L**. It also revealed that the peaks associated with two CH=N carbons at δ 161.73 ppm had vanished, while two additional carbons (CH2N) (Ref. 21) had appeared at δ 48.72 ppm. Table 1 shows that the ligand has a lower melting point than the colourful crystalline powder that is the platinum complex. It is stable at high temperatures and dissolves easily in common solvents such ethanol, dimethylformamide, and dimethyl sulphoxide. In comparison to their predicted values, the substances' atomic absorption spectrometry findings were approximations.

**Table 1**. Physical properties of (**L**) and platinum complex

| Compound | Colour | Molecular weight | Melting point (°C) | Found (Calc.) (%) | | | | | $\Lambda_M$ ($cm^2$ $\Omega^{-1}$ $mol^{-1}$) |
|---|---|---|---|---|---|---|---|---|---|
| | | | | M | C | H | N | Cl | |
| (**L**) | brown | 458.64 | 167°C | – | 62.92 | 10.25 | 6.33 | – | – |
| $C_{24}H_{46}N_2O_6$ | | | | | (62.85) | (10.11) | (6.11) | | |
| Pt(II)-Complex | brown | 722.61 | 220–222 °C | 27.33 | 39.61 | 6.09 | 3.94 | 9.65 | 19.25 |
| $C_{24}H_{44}C_{l2}N_2O_6Pt$ | | | | (27.00) | (39.89) | (6.14) | (3.88) | (9.81) | |

M – Atomic absorption.

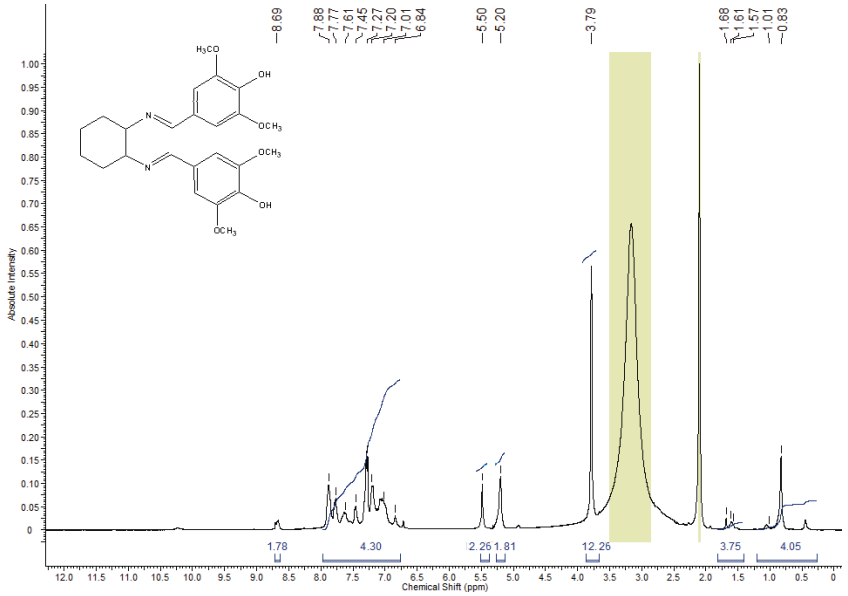


**Fig. 2**. [1]H NMR spectrum of compound **P**

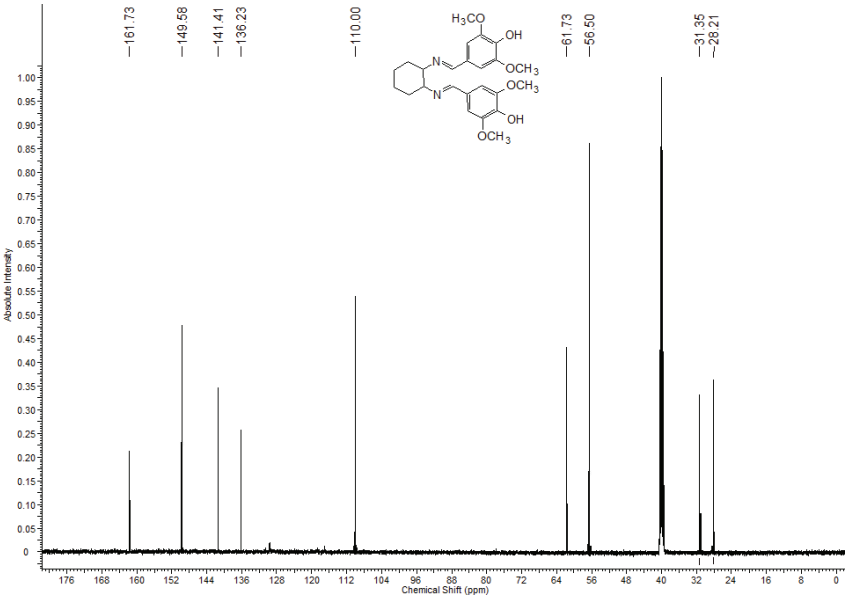


**Fig. 3**. [13]C NMR spectrum of compound **P**

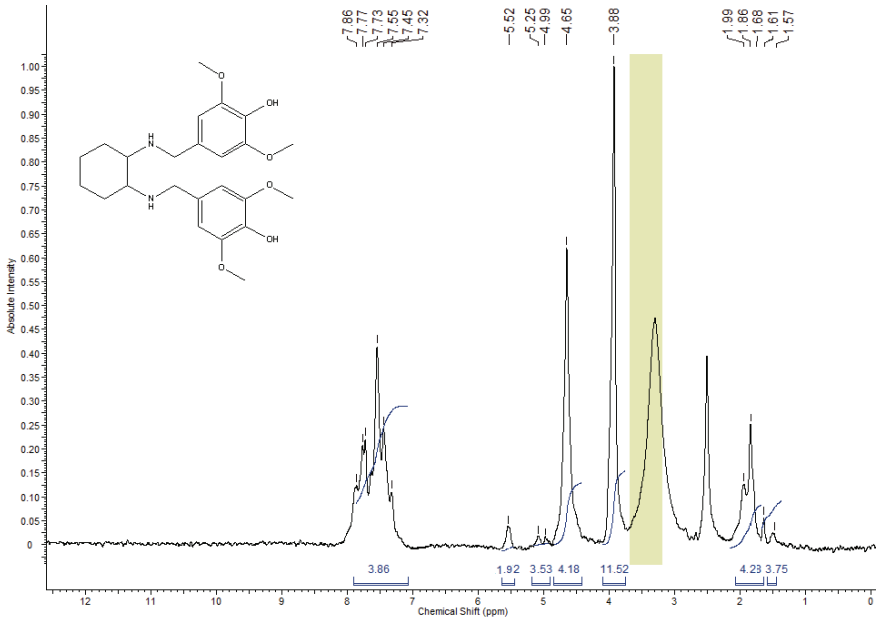


**Fig. 4**. [1]H NMR spectrum of compound **L**

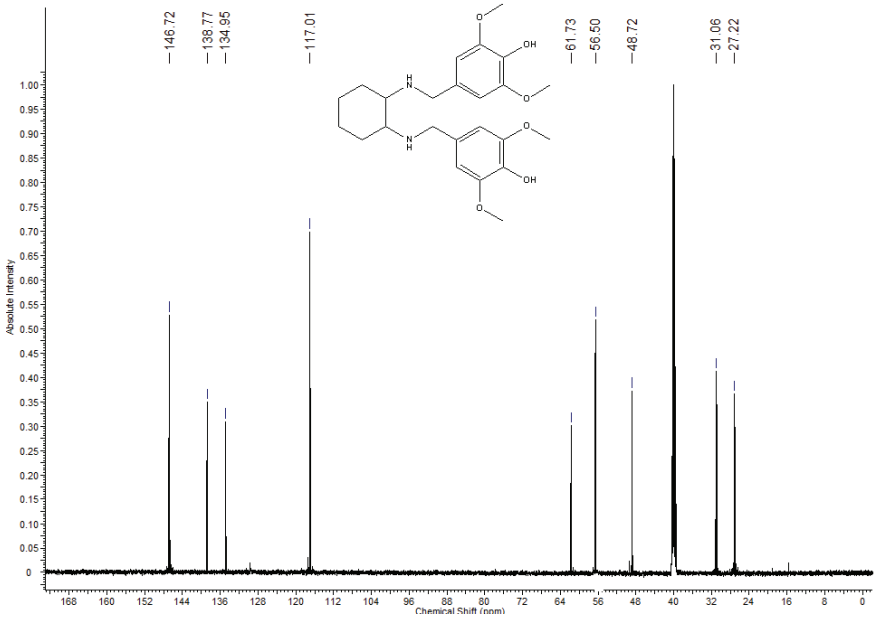


**Fig. 5**. [13]C NMR spectrum of compound **L**

Table 2 and Fig. 6 show the FTIR spectra of the prepared compounds and the locations of the significant bands of the compounds that were produced. When com-

plexed, the ligand (**L**) showed distinctive ϕ(N–H) stretching frequencies at (3324) $cm^{-1}$, which shifted to higher frequencies at (3411) $cm^{-1}$. This proves that amine nitrogen is involved in the bonding process. The debut of additional bands at (492), (530) and (323) $cm^{-1}$, which are assigned to υ (M-N), υ (M-O), and υ (M-Cl), correspondingly, validates the suggested coordination locations. In the spectrum of Pt(II), the presence of a shower of bands in the region of (835) $cm^{-1}$, which corresponds to ρ($H_2O$), validates the coordination of water with the core ion[22,23].

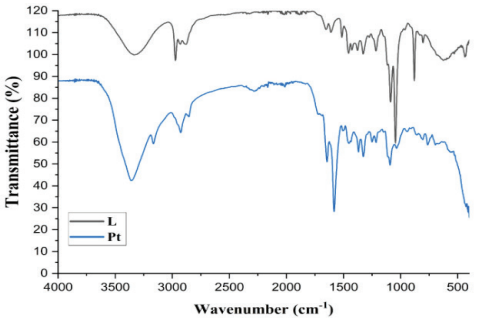


**Fig. 6**. FTIR spectra of **L** and the platinum complex

**Table 2**. FTIR analysis results for the synthesised chemicals ($cm^{-1}$)

| Compound | υ(N–H) amine | υ(M–N) | υ(M–O) | υ(M–Cl) | ρ($H_2O$) |
|---|---|---|---|---|---|
| Ligand (**L**) | 3324 | – | – | – | – |
| Pt complex | 3411 | 492 | 530 | 323 | 835 |

The electronic transitions associated with the prepared compounds for ligand **L** and the platinum complex are listed in both Table 3 and Fig. 7, noting the differences occurring between them, which confirm the coordination[24,25].

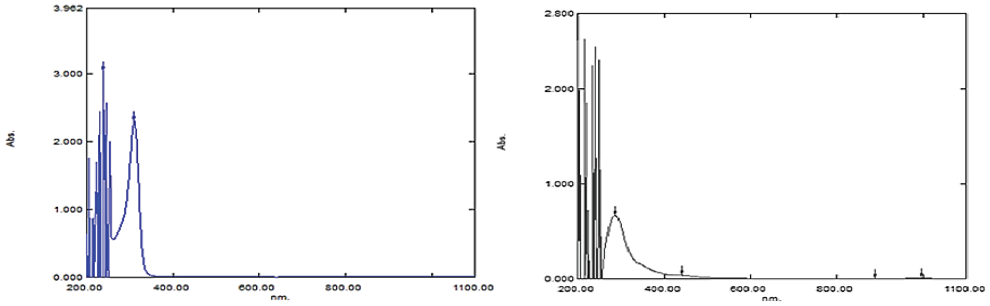


(A) (B)

**Fig. 7**. Electronic spectra for ligand **L** (A) along with the platinum complex (B)

**Table 3**. Electronic transfer data for **L** and the platinum complex

| Compound | Wavenumber | | Transitions | Geometric structure | $\mu_{eff}$ B.M. |
|---|---|---|---|---|---|
| | nm | $cm^{-1}$ | | | |
| Ligand (**L**) | 313 | 31948 | $n \rightarrow \pi^*$ | – | – |
| | 238 | 42016 | $\pi \rightarrow \pi^*$ | | |
| Pt complex | 635 | 15748 | $^1A_1g \rightarrow {}^3T_1g$ | octahedral | 0 |
| | 528 | 18939 | $^1A_1g \rightarrow {}^3T_2g$ | | |
| | 422 | 23696 | C.T | | |

C.T. – Charge Transfer; B.M.= Bohr magneton.

## EFFECT OF CONCENTRATION AND TEMPERATURE

Findings from the weight loss experiment showed that inhibitory efficacy rose with increasing concentrations of inhibitors but fell with increasing temperatures. At 298 K, maximum inhibition (97.5%) was achieved at 700 ppm. The decline in efficiency at higher temperatures suggests that adsorption was primarily physical in nature. The second occurrence might be due to the inhibitor's more effective surface adsorption or to the inhibitor's complete coating of the copper surface[26,27].

The corrosion and inhibitor effectiveness speeds (SP) were recorded after 3 h of immersion in a 0.5 M $HNO_3$ solution (Table 4). The experiments were conducted at various temperatures, with and without the inhibitor.

**Table 4**. Corrosion and inhibitor effectiveness speeds (SP) after 3 h of immersion in a 0.5 M $HNO_3$

| Temperature | $C_{inh}$ (ppm) | CR (mdd) | θ | η (%) |
|---|---|---|---|---|
| 298 K | Blank | 46.32 | – | – |
| | 500 | 5.09 | 0.890 | 89.0 |
| | 600 | 3.47 | 0.925 | 92.5 |
| | 700 | 1.65 | 0.977 | 97.7 |
| 308 K | Blank | 85.60 | – | – |
| | 500 | 10.264 | 0.88 | 88.0 |
| | 600 | 7.5 | 0.912 | 91.2 |
| | 700 | 3.16 | 0.963 | 96.3 |
| 318 K | Blank | 115.8 | – | – |
| | 500 | 19.687 | 0.829 | 82.9 |
| | 600 | 12.73 | 0.89 | 89.0 |
| | 700 | 6.95 | 0.94 | 94.0 |
| 328 K | Blank | 184.13 | – | – |
| | 500 | 34.74 | 0.811 | 81.0 |
| | 600 | 22.87 | 0.878 | 87.8 |
| | 700 | 15.22 | 0.917 | 91.7 |

mdd – ml/density$^2$ day.

Corrosion inhibition efficacy decreased as CR levels increased with rising temperatures, as seen in Table 4. Physical adsorption on the copper alloy surface is clearly shown by the shifting of equilibrium points from "absorption/desorption," where "desorption" is the dominant term. We used the Arrhenius equation to determine the activation energy $E_a$ (Ref. 8):

$$\log \mathrm{CR} = -E_a/(2.303\ R\ T + \log A), \tag{4}$$

where $E_a$ is the activation energy, the gas constant – by $R$ (8.314), and the Arrhenius constant – by $A$. The experimental findings corroborate the hypothesis that the linear relation would be reached by graphing log (CR) versus $1/T$, which is given by equation (4). At $T = 0$, when the extrapolated line meets, we get log $A$ and the slope of the line gives the value of $-E_a/R$ (Ref. 14).

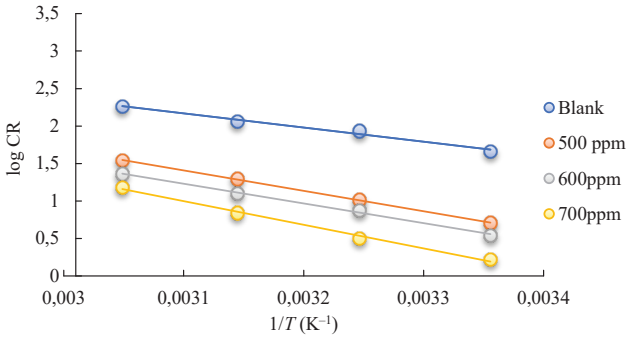


**Fig. 8**. The Arrhenius curves of log CR versus $1/T$ for the corrosion of copper alloy in 0.5 M $HNO_3$ without and with different dosages of inhibitor

The values of $\Delta H$ and $\Delta S$ may be calculated using equation (5), which is an alternate version of the Arrhenius relationship:

$$\ln (I_{corr}/T) = \ln (R/(N\,h)) + (\Delta S*/R) - (\Delta H*/RT) \tag{5}$$

where $N$ is the Avogadro number, equal to $6.022 \times 10^{23}$ molecules per mol, and $h$ – the Planck's constant, equal to $6.626 \times 10^{-34}$ J s. The slope of the straight line of ($\ln I_{corr}/T$) versus $1/T$ depicts its magnitude ($\Delta H^*/R$) and the intersection depicts its magnitude ($\ln R/(N\,h) + \Delta S*/R$). The consequences are explained in Table 5 and Figs 8 and 9 (Ref. 28).

**Table 5**. Values of activation energy ($E_a$), enthalpy ($\Delta H$) and entropy ($\Delta$S) for copper alloy corrosion in 0.5 M in the presence and absence of inhibitor

| Concentration (M) | $E_a$ (kJ mol$^{-1}$) | $\Delta H$ (kJ mol$^{-1}$) | $-\Delta S$ (J mol$^{-1}$ K$^{-1}$) |
|---|---|---|---|
| Blank | 36.1655 | 33.56685464 | 77.60336653 |
| 500 ppm | 52.1489 | 48.79649139 | 62.19757607 |
| 600 ppm | 54.1022 | 54.29555057 | 45.96462909 |
| 700 ppm | 60.3548 | 58.92150008 | 33.16476466 |

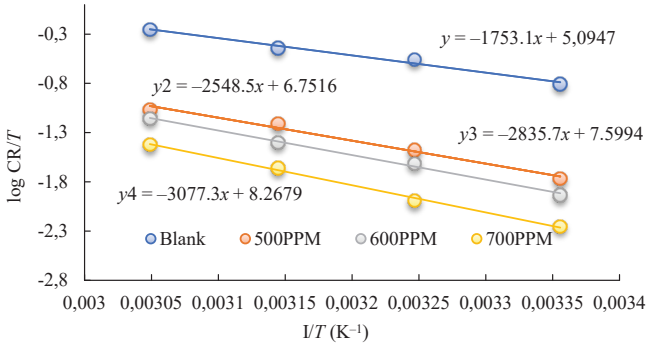


**Fig. 9**. A plot of logto 1/*T* for the corrosion of copper alloy in 0.5 M $HNO_3$ in the presence and absence of diverse concentrations of inhibitor at 4 temperatures ranging from 298 to 328K

Along with proving that inhibitor molecule adsorption on Cu surfaces is physical, the fact that the activation energy $E^*_a$ increases as inhibitor concentrations suggests that the energy barrier for the corrosion process also increases. Because of the non-linear relationship between the Arrhenius coefficient and activation energies, corrosion processes often start at low-energy sites and move to higher-energy ones.

*Adsorption isotherm*. Adsorption of inhibitors on metal surfaces is broadly classified into two interactions, physisorption and chemisorption, based on the size (molecular structure) of the inhibitor, the type of electrolyte (corrosion medium), and the elements (charge and properties) of the corroding metal. One of the essential components of discussions involving adsorption properties as measured by adsorption isotherms is average data. The process of inhibitory molecule binding and interaction with metal surfaces is detailed. The adsorption isotherm explains the ideal Langmuir isotherm and is a valuable tool for analysing the impact of surface coverage (θ) and inhibitor solution concentration ($C_{inh}$) on inhibitor[30]:

$$C_{inh}\,\theta = 1/K_{ads} + C_{inh} \tag{6}$$

$$\Delta G^{o}_{ads} = -RT \ln (55.5\, K_{ads}), \tag{7}$$

where $K_{ads}$ is adsorption/desorption equilibrium constant suggesting which inhibitor molecules have been approaching the surface adsorption positions. Then, the measured $K_{ads}$ stands for computing Gibbs free energies for adsorption through adsorption parameters and are listed in Table 6 (Refs 31 and 32).

$$\ln (i_{corr}\, T) = \ln (R\, N\, h) + (\Delta S_{act}\, R) - (\Delta H_{act}\, RT).$$

Typically, when electrostatic contact occurs, the $\Delta G_{ads}$ values may go as low as –20 kJ/mol. The reason the $\Delta G_{ads}$ values are more than –40 kJ/mol is because inhibitor molecules charge metal surfaces or establish coordinate covalent bonds (chemisorption). Confirming inhibitor molecule monolayer adsorption on copper, the adsorption results were in good agreement with the Langmuir adsorption isotherm (Fig. 10). According to Langmuir adsorption isotherm, the protective layer is created when

molecules of inhibitor are adsorbed onto the surface of the copper. This results in the copper being covered with the platinum complex. When there was a higher quantity of the inhibitor, the protection that was afforded by it was also of a higher quality. The maximal value reaches 97.7% at 700 ppm of inhibitor and 298 K.

Inhibitor characteristics of physical adsorption were shown by computed Gibbs free energies of adsorption ($\Delta G°_{ads}$) ranging from –13.956 to –16.863 kJ/mol values (Fig. 11). The endothermic nature of the adsorption process was supported by positive enthalpy values ($\Delta H°_{ads}$), and the decreased randomness at the metal-solution interface was verified by the corresponding negative entropy values ($\Delta S°_{ads}$).

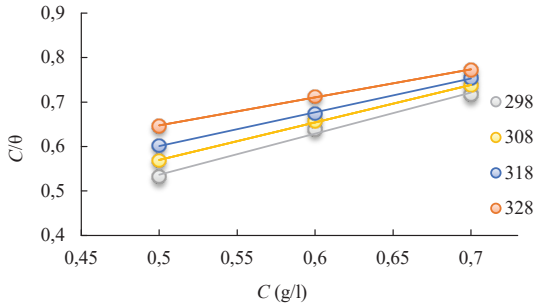


**Fig. 10**. Langmuir isotherm curves for inhibitor adsorption for copper in 0.5 M $HNO_3$

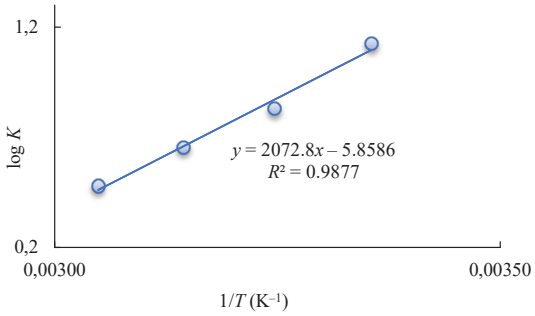


**Fig. 11**. Plot of log $K_{ads}$ versus $1/T$ based on carbon steel corrosion in 0.5 M $HNO_3$ solution in the absence and in the presence of inhibitor at diverse temperatures

**Table 6**. Thermodynamic equations for adsorption of inhibitor on copper in 0.5 M $HNO_3$

| Temperature (K) | $K_{ads}$ | $-\Delta G_{ads}$ (kJ mol$^{-1}$) | $\Delta H_{ads}$ (kJ mol$^{-1}$) | $-\Delta S_{ads}$ (J mol$^{-1}$ K$^{-1}$) |
|---|---|---|---|---|
| 298 | 13.332 | 16.368 | 39.6881 | 85.0528 |
| 308 | 6.7586 | 15.177 | | |
| 318 | 4.5210 | 14.608 | | |
| 328 | 3.0080 | 13.956 | | |

**Table 7**. Comparison table between platinum-urea complexes and organic materials in terms of their use as metal corrosion inhibitors **– cite and discuss in the text!!!**

| Property | Palladium complexes (Pt complexes) **??? or Platinum** | Urea | Benzotriazole (BTA) | Amino Acids |
|---|---|---|---|---|
| Corrosion inhibition efficiency | Very high (often >90%) | Low to moderate | Very high, especially for copper and its alloys | Moderate to high |
| Inhibition mechanism | Adsorption and formation of a stable protective complex film on the metal surface | Weak physical and chemical adsorption | Formation of a strong protective film and stable complexes with copper | Adsorption through amino (–$NH_2$) and carboxyl (–COOH) functional groups |
| Thermal stability | Excellent | Moderate | Good to excellent | Moderate to high |
| Metal selectivity | Can be tailored for specific metals | Low selectivity | Excellent for copper and copper alloys | Good for various metals |

*Surface morphology*. SEM analysis revealed severe surface damage and roughness on copper samples exposed to uninhibited $HNO_3$ solution (Fig. 12). In contrast, specimens treated with 700 ppm inhibitor, displayed a smoother surface, confirming a protective inhibitor layer creation.


A

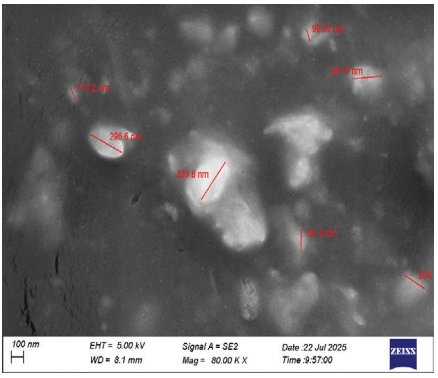


B

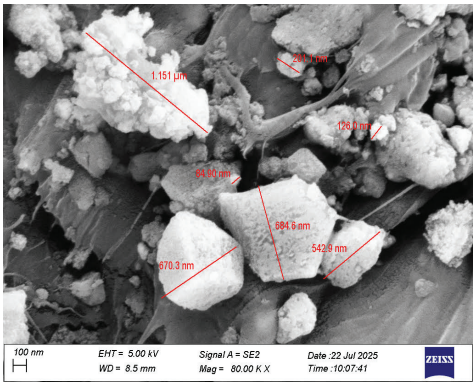


C

**Fig. 12**. SEM images of purified Cu alloy – A, Cu alloy dipped in 0.5 M $HNO_3$ – B, and Cu alloy immersed in 0.5 M $HNO_3$ containing 700 ppm inhibitor – C

## CONCLUSIONS

In this study, elemental analyses, M%, UV-Vis, FT-IR, and $^{1}H$,$^{13}C$-NMR measurements were used to construct and depict ligand (**L**) complexes formed. Its octahedral structure has been confirmed by magnetic susceptibility measurements. Results showed that in 0.5 M $HNO_3$ solutions, platinum complex effectively inhibited copper, suggesting that this compound may have applications beyond weight reduction.

## ACKNOWLEDGEMENTS

For their unwavering scientific backing during the study period, the authors extend their deepest gratitude to the Department of Chemistry, laboratory staff, and the esteemed academics.

## REFERENCES

1. S. A. SAOUD, D. F. HUSSAIN, R. M. SHAKIR: Synthesis, Antibacterial, and Molecular Docking Study of Novel 2-Chloro-8-methoxy-3-aryl-[1,3] Benzoxazine Derivatives Using Vilsmeier Reagent. Technology, **10** (3), 487–498 (2020).
2. R. M. SHAKIR, S. A. SAOUD, H. S. JASIM, D. F. HUSSAIN: Synthesis, Antioxidant Activity and Molecular Docking Study of 1,2,4-Triazole and Their Corresponding Fused Rings Containing 2-Methylphenol. IJDDT, **11** (2), 501–511 (2021).
3. M. ENIKEEV, D. POTEMKIN, L. ENIKEEVA et al.: Analysis of Corrosion Processes Kinetics on the Surface of Metals. Chem Eng J, **383**, 123131 (2020).
4. H. S. HASSAN, K. H. RASHID, K. F. AL-AZAWI, A. A. KHADOM: A Combined Experimental and Theoretical Study into the Effect of New Heterocyclic Compound Containing β-Lactam Ring as Corrosion Inhibitor for Mild Steel in Hydrochloric Acid. Results Surf Interfaces, **17**, 100319 (2024).
5. A. M. AL-GHABAN, H. A. ABDULLAH, R. A. ANAEE, S. A. NASER, A. A. KHADOM: Expired Butamirate Drug as Eco-friendly Corrosion Inhibitor for Aluminum in Seawater: Experimental and Theoretical Studies. J Eng Res, **12** (3), 299–309 (2024).

6. S. SAOUD, S. HABEEB, M. ALI, H. ALMASHHADANI: Synthesis of Bis Chromene Derivative as a Dual-functional Corrosion Inhibitor and CDK2 Targeting Agent. Int J Corros Scale Inhib, **14** (2), 905–929 (2025).
7. Y. QIANG, S. ZHANG, S. XU, L. YIN: The Effect of 5-Nitroindazole as an Inhibitor for the Corrosion of Copper in a 3.0% NaCl Solution. RSC Adv, **5** (78), 63866–63873 (2015).
8. Y. QIANG, S. ZHANG, S. XU, W. LI: Experimental and Theoretical Studies on the Corrosion Inhibition of Copper by Two Indazole Derivatives in 3.0% NaCl Solution. J Colloid Interface Sci, **472**, 52–59 (2016).
9. J. ZHANG, Z. LIU, G.-C. HAN, S.-L. CHEN, Z. CHEN: Inhibition of Copper Corrosion by the Formation of Schiff Base Self-assembled Monolayers. Appl Surf Sci, **389**, 601–608 (2016).
10. A. M. A. AL-KHAZRAJI, E. J. WAHEED, A. A. R. AHMED: Synthesis of CuO Nanoparticles from Copper (II) Schiff Base Complex: Evaluation via Thermal Decomposition. Indones J Chem, **25** (1), 50–59 (2024).
11. H. F. EMRAYED, E. A. AMRAGA, D. M. IBRAHIM, A. E.-A. S. FOUDA: Corrosion Inhibition Effect of Schiff Base and Its Metal Complexes with [Mn (II) and Cu (II)] on Carbon Steel in Hydrochloric Acid Solution: Experimental and Surface Studies. Int J Electrochem Sci, **20** (1), 100912 (2025).
12. H. S. MANDOUR et.al.: Exploring Corrosion Behavior, Antimicrobial Evaluation, Molecular Docking and DFT Calculation of Thiosemicarbazone Ligand and Its Metal Complexes. Scientific Reports, **15** (1), 16577 (2025).
13. A. S.MAHDI: Amoxicillin as Green Corrosion Inhibitor for Concrete Reinforced Steel in Simulated Concrete Pore Solution Containing Chloride. International Journal of Advanced Research in Engineering and Technology, **5**, 99–107 (2014).
14. E. H. ALI, T. A. HIMDAN, Z. W. AHMED: Gallic Acid as Corrosion Inhibitor for Aluminum 6061 in Alkali Solutions. Ibn Al-Haitham Journal for Pure and Applied Sciences, **32** (1), 17–27 (2019).
15. R. M. SHAKIR et al.: Synthesis, Antioxidant, Antibacterial and Docking Structure of New Dihydro-Pyrimidine Derivatives Containing Multi Phenol. J Pharm Negat Results, **13** (2), 57 (2022).
16. R. M. SHAKIR et al.: Synthesis, Antioxidant ability and Docking Study for New 4, 4'-((2-(Aryl)-1H-benzo[d]imidazole-1,3(2H)-diyl)bis(methylene)) Diphenol. Res J Chem Environ, **26** (10), 10 (2022).
17. E. J. WAHEED: Synthesis, Characterization and Anticancer Activity of Some Metal Complexes of New Ligand Derived from 4-Methylbenzohydrazide with Computational Studies. Iraqi J Pharm Sci, **34** (2), 122–143 (2025).
18. E. J WAHEED: Synthesis, Spectral Characterization, DNA Cleavage, and Antioxidant Properties of Metal Complexes with a Novel Schiff Base Ligand Derived from 4-Chlorobenzoic Acid. Iraqi J Sci, **66** (7), 2669–2691 (2025).
19. Z. W. AHMED, M. A. QASEM: Protective Effect of Expired Drug on Corrosion of Copper in Acidic Medium. Wasit J Pure Sci, **2** (2), 215–230 (2023).
20. M. A. KADHIM, M. A. EL-HASHASH, S. A. RIZK: Facile Synthesis, Characterization of Novel Schiff Bases and N-Nucleosides Bearing Quinazoline Moiety and Evaluation Their Antimicrobial Effects. Journal of University of Anbar for Pure Science (JUAPS), **16** (1), 13–19. (2022).
21. H. S. ADEEB, S. S. ABED SAOUD: Synthesis, Characterization, Antimicrobial Activity, and Docking Study of Some 1, 3, 4-Oxadiazole Derivatives with Tert-amine Moiety. Iran J Chem Chem Eng, **43** (9), 3221–3236 (2024).
22. E. J. WAHEED: Synthesis, Characterization and Biological Activity of New Ligand Derived from 4-(Dimethylamino) Benzaldehyde and Nano Copper Complex. Baghdad Sci J, **22** (4), 1085–1101 (2025).
23. S. A. HASSAN, S. M. LATEEF, I. Y. MAJEED: Structural, Spectral and Thermal Studies of New Bidentate Schiff Base Ligand Type (NN) Derived from Mebendazol and 2-Aminobenzothaizol and Its Metal Complexes and Evaluation of Their Biological Activity. J Glob Pharma Technol, **10** (07), 307–317 (2018).

24. Z. HUSSAIN, K. A. SALEH: Electrochemical Study of Inhibition for Low Carbon Steel Corrosion in the Saline Medium through a Novel Polymer-Metal Oxides Nanocomposite. Iraqi J Sci, **66** (4), 1463-1477 (2025).
25. A. FAWZY et al.: Investigation of Transition Metal Chelates with a Ligand (3-Cyano-6-thiophen-2-yl [4, 4′] Bipyridinyl-2-yloxy)-acetic Acid Hydrazide as Corrosion Inhibitors for Copper in 1.0 M HCl Solution. Int J Electrochem Sci, **18** (7), 100189 (2023).
26. M. A. ALI, A. M. OUF, A. EL-HOSSIANY, A. FOUDA: Eco-friendly Approach to Corrosion Inhibition of Copper in $HNO_3$ Solution by the Expired Tylosin Drug. Biointerface Res Appl Chem, **12** (4), 5116–5130 (2022).
27. F. WEDIAN, M. A. AL-QUDAH, G. M. AL-MAZAIDEH: Corrosion Inhibition of Copper by *Capparis spinosa* L. Extract in Strong Acidic Medium: Experimental and Density Functional Theory. Int J Electrochem Sci, **12** (6), 4664–4676 (2017).
28. K. F. AL-AZAWI et al.: Synthesis and Characterization of (E)-4-(((4-(5-mercapto-1, 3, 4-oxadiazol-2-yl) phenyl) amino) methyl)-2-methoxyphenol as a Novel Corrosion Inhibitor for Mild-steel in Acidic Medium. Results Chem, **5**, 100975 (2023).
29. Z. W. AHMED, J. NASER, A. FAROOQ: Inhibition of Aluminum Alloy 7025 in Acid Solution Using Sulphamethoxazole. Egypt J Chem, **63** (10), 3703–3711 (2020).
30. Z. W. AHMED, E. H. ALI, I. M. RADHI: Corrosion Protection of Carbon Steel in Saline Solution Using Plant Extracts. Int J Pharm Res, **Jan – Jun 2020** (Supl.1), 2078–2086 (2020),
31. E. H. ALI, J. A. NASER, Z. W. AHMED, T. A.HIMDAN: Corrosion Protection of 5083 AA in Saline Water by Polyacrylonitrile Nano Fibers. J Renew Mater, **9** (11), 1927–1939 (2021).
32. Z. W AHMED, A. A.KHADOM, E. H.ALI, K. F.AL-AZAWI, A. AH.KADHUM: Expired Azithromycin and Cephalexin as Corrosion Inhibitors for Aluminum in Saline-Acidic Solution. S Afr J Chem Eng, **53** (1), 193–201 (2025).

*Received 28 April 2026*
*Accepted 21 July 2026*